Ultrafast dynamics of gas-phase excited-state intramolecular proton transfer in 1-hydroxy-2-acetonaphthone

ARTICLE *in* CHEMICAL PHYSICS LETTERS · AUGUST 1999

Impact Factor: 1.9 · DOI: 10.1016/S0009-2614(99)00717-4

4 AUTHORS, INCLUDING:

I-Ren Lee
National Taiwan Normal University
16 PUBLICATIONS **318** CITATIONS

27 August 1999

ELSEVIER

Chemical Physics Letters 310 (1999) 103–110

CHEMICAL PHYSICS LETTERS

www.elsevier.nl/locate/cplett

Ultrafast dynamics of gas-phase excited-state intramolecular proton transfer in 1-hydroxy-2-acetonaphthone

Chengii Lu, Re-Ming R. Hsieh, I-Ren Lee, Po-Yuan Cheng *

Department of Chemistry, National Tsing Hua University, Hsinchu, 30043, Taiwan

Received 8 June 1999

Abstract

The excited-state dynamics of 1-hydroxy-2-acetonaphthone (HAN) was studied in the gas phase using femtosecond time-resolved multiphoton ionization spectroscopy. Following femtosecond excitation to its S_1 state, HAN was found to exhibit a biexponential decay behavior which can be consistently interpreted in terms of rapid excited-state intramolecular proton transfer (ESIPT) followed by other slower decay channels. The results revealed that ESIPT in HAN (S_1) occurs in $\sim$ 60–85 ps in the energy range studied and suggested the existence of an energy barrier to tautomerization. © 1999 Elsevier Science B.V. All rights reserved.

1. Introduction

The excited-state intramolecular proton (or hydrogen) transfer (ESIPT) is one of the most fundamental photochemical reactions and plays an important role in many chemical and biological processes [1,2]. ESIPT usually occurs in molecules with intramolecular hydrogen bonding and proceeds by excitation of the 'normal' form followed by rapid proton (or hydrogen) transfer in the excited state to its tautomeric configuration [3]. Since the seminal work of Weller [4] on the ESIPT of methyl salicylate, ESIPT in a variety of molecular systems have been the focus of research interests for several decades [2,3,5]. Most time-resolved studies of ESIPT reported so far were conducted in condensed phases, and recently direct time-resolved studies of ESIPT in the gas phase have been made [6]. Although the condensed-phase studies have revealed the importance of solvation to the ESIPT dynamics, the coupling of reaction coordinates to the solvent bath modes may complicate and smear the dynamical features [7]. In this Letter, we report femtosecond time-resolved studies of gas-phase ESIPT in 1-hydroxy-2-acetonaphthone (HAN). This molecule is the naphthalene analogue of *o*-hydroxybenzaldehyde (OHBA) and other related compounds, which can be regarded as prototypes for ESIPT due to their relative structural simplicity.

The first absorption band of HAN in the static vapor phase is located between 310 and 410 nm and is quasi-continuous due to thermal congestion [8]. It has been assigned to the excitation to the lowest S_1 (π, π^*) state of the planar conjugated system including the chelate pseudo-aromatic ring [9]. Several

* Corresponding author. Fax: +886-3-5711082; e-mail: pycheng@chem.nthu.edu.tw

0009-2614/99/$ - see front matter
PII: S0009-2614(99)00717-4

spectroscopic studies of HAN have been reported in view of its ESIPT. Catalán and del Valle [8] measured the absorption and fluorescence spectra of HAN in solutions and in the vapor phase. Based on the observation of a relatively small Stokes shift (~ 6000 cm^{-1}) of the single fluorescence band, they concluded that ESIPT does not occur in HAN. Douhal et al. [9] studied HAN isolated in a free jet. They found that the S_1–S_0 fluorescence excitation spectrum is well resolved until 900 cm^{-1} above the origin at 388.6 nm. Emission from the vibrationless level of the S_1 state exhibits a dual character; the short-wavelength fluorescence is highly structured, while the long-wavelength part (~ 2200 and 3500 cm^{-1} red-shifted from the origin) is more intense and diffuse. The fluorescence lifetimes of the two bands were found to be identical (9.3 ns). They ascribed these observations to rapid ESIPT from the initial enol form to the tautomeric keto form through a small energy barrier. Recently, Tobita et al. [10] studied HAN and two other related compounds, methyl 1-hydroxy-2-naphthoate (1H2MN) and 1-hydroxy-2-naphthaldehyde (1H2NA), in cyclohexane solutions. The Stokes shifts observed for HAN and 1H2NA (~ 6000 cm^{-1}) were found to be much greater than that observed for 1H2MN (~ 3400 cm^{-1}). These observations and other evidences have led them to conclude that ESIPT does occur in both HAN and 1H2NA.

Hence, although some controversies exist, these previous frequency-resolved studies seem to suggest that ESIPT occurs in HAN in liquid solutions as well as in the gas phase. Although the free-jet ns fluorescence study [9] has revealed the essential features of the ESIPT dynamics in HAN, the rapid proton transfer itself was not resolved due to the insufficient time resolution (~ 6 ns) used. With femtosecond (fs) time resolution, this rapid ESIPT process should be resolvable. In the present study, we employed femtosecond time-resolved multiphoton ionization spectroscopy to investigate the excited-state dynamics in HAN. Similar techniques have been utilized to study non-dissociative dynamics involving molecular configuration change such as isomerization [11,12], double proton transfer [13] and twisted intramolecular charge-transfer [14]. Our results revealed the ultrafast nature of the excited-state dynamics in HAN and are consistent with rapid ESIPT occurring in its S_1 state.

2. Experimental

The laser system employed in this work consists of a self-mode-locked Ti:sapphire laser oscillator (Spectra-Physics, Tsunami) and a chirp-pulse regenerative amplifier (Spectra-Physics, Spitfire). The oscillator produced 82 MHz, ~ 80 fs pulse trains with an average power of ~ 1 W around 800 nm. These pulses were selected and amplified through the stretcher, regenerative amplifier and compressor stages, producing 1 kHz fs pulses of ~ 1 mJ/pulse in energy and ~ 120 fs in duration. The output wavelength of this system is tunable from 760 to 840 nm. The amplifier output was split into two parts by a 50/50 beamsplitter. The transmitted beam was frequency-doubled in a 200 μm thick BBO crystal to produce the pump pulses at ~ 400 nm, while the reflected pulses were sent to a computer-controlled optical delay line and were used as the probe pulses. The irradiance of the pump and probe pulses was adjusted by placing neutral density filters in their beam paths. A half-wave plate and polarizer combination was also placed in the probe beam path to rotate and ensure its polarization. For the results presented here, the polarization of the probe laser was set at the magic angle (54.7°) with respect to that of the pump laser. The pump and probe beams were then recombined collinearly via a dichroic mirror and were focused into a photoionization cell using an $f = 200$ mm lens. The cross correlation of the pump and probe pulses was $\sim 200 \pm 20$ fs FWHM as measured by sum-frequency generation before entering the cell.

The photoionization cell is made of stainless steel and has a sample tube containing HAN crystals connected to it. The HAN vapor was allowed to diffuse freely into the cell which was continuously evacuated to maintain a total pressure of ~ 10 mTorr. The sample tube was maintained at ~ 30°C, while the cell body and the entrance windows were kept at 45°C and 60°C, respectively, to minimize deposition of solid HAN on the surfaces. The laser beams entered the cell through a quartz window and were focused and spatially overlapped between a pair of electrodes which were biased at ~ 80 V (15 mm apart) to collect the ions and electrons. The transient current created by the laser pulses was amplified by a current amplifier and the output was sent to a gated

integrator and averager for signal processing. The transients were obtained by monitoring the integrated current while the pump vs. probe delay time was scanned.

3. Results and discussion

The dynamics of the HAN S_1 state was probed at three excitation wavelengths (410, 397 and 385 nm) near the red tail of its S_1–S_0 absorption band. Figs. 1 and 2 show the results of the short-time and long-time scans taken at these wavelengths in a $\sim$45°C HAN vapor. The pump and probe pulse energies were kept at minimal levels to avoid interference from the upper excited states. As shown in Fig. 1, these transients exhibit an extremely fast initial decay, hereinafter referred to as the 'initial spike', around the zero delay time followed by a much slower temporal feature. Transients taken at parallel and perpendicular pump–probe polarizations show additional features on a time scale of a few picoseconds (ps) which can be attributed to rotational dephasing [15]. Although interesting in its own right, this rotational coherent effect is not the focus of the present study and we set the relative pump–probe polarization at the magic angle (54.7°) to produce unmodulated population transients [15].

The initial spike exhibits a symmetric profile resembling the system time response function (FWHM $\sim$ 200 fs) and cannot be resolved with any meaningful time constants. An experimental trace of the pump–probe cross-correlation function is shown in Fig. 1(c) for comparison. This indicates that the initial spike is associated with a nearly instantaneous process. As shown in Fig. 1, the amplitude ratio of the initial spike to the long-time decay depends strongly on the excitation wavelength. As the excitation wavelength increases, the initial spike amplitude remains nearly unchanged while the long-time component decreases. Comparing with the HAN gas-phase absorption spectrum shown in Fig. 1(a) inset, one finds that the excitation wavelength dependence of the long-time component amplitude is qualitatively consistent with the HAN S_1–S_0 absorption in this spectral region. On the contrary, the initial spike is rather wavelength independent. In fact, the initial spike can be observed with similar intensities even at

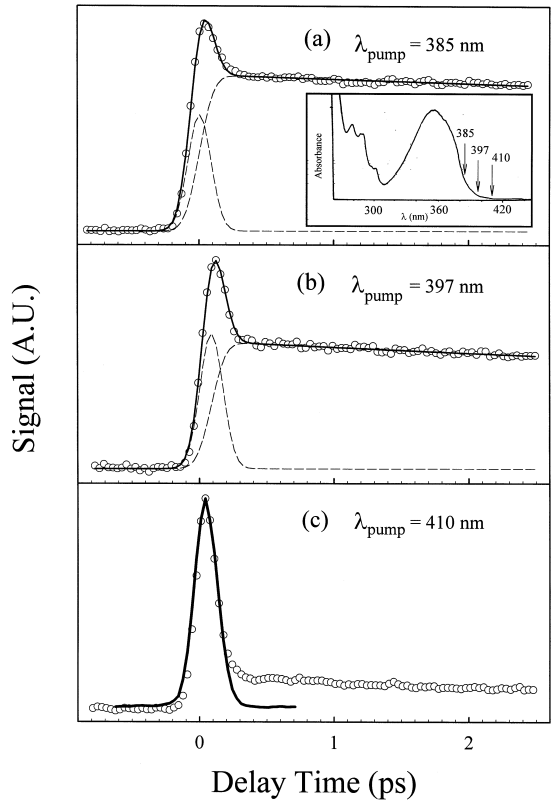

Fig. 1. Early-time transients of HAN excited at three pump wavelengths: (a) 385 nm, (b) 397 nm and (c) 410 nm. The inset in (a) is an absorption spectrum of HAN vapor in a static cell at 368 K (adopted from Ref. [8]). The pump and probe pulse energies used here were $\sim$1 and $\sim$10 μJ/pulse, respectively. The open circles are the experimental data. The thin solid lines in (a) and (b) are results of nonlinear least-square fits to a sum of a delta function and a single exponential decay convoluted with the 200 fs FWHM Gaussian response function. The dashed lines represent the decomposition of the total signal into these two components as obtained from the fits. The thick solid line in (c) is an experimental trace of the pump–probe cross correlation superimposed on top of the transient for comparison. The three transients have been normalized to the same maximum intensity for easy comparison.

excitation wavelengths longer than 420 nm where the HAN absorption is practically absent. To further clarify the origin of the initial spike and the long-time decay, we have also studied their laser irradiance dependence. Around the typical pump pulse energy used ($\sim$1–5 μJ/pulse), the long-time decay was found to depend linearly on the pump laser irradiance through the entire scanned range. On the other hand, the initial spike exhibits a larger dependence of

~ 1.5, indicating a combination of one- and two-photon transitions. Based on these observations, we assigned the long-time decay to the S_1-state dynamics and the initial spike to the two-color coherent multiphoton absorption processes occurring only at zero delay time. A small component hidden in the initial spike due to the extremely fast initial wave packet dephasing in the S_1 state is also possible but can not be resolved. Thus, the initial spike is considered to be irrelevant to the S_1-state dynamics except for the possible initial dephasing and we will only focus on the long-time decay in the following discussion.

The long-time decay exhibits a prominent non-exponential behavior as shown in Fig. 2. These transients can be consistently explained on the basis of the mechanism proposed by Douhal et al. [9]. As schematically illustrated in Fig. 3, HAN is first excited to the S_1 state in its enol configuration, hereinafter denoted as E^*, by the pump pulse. By crossing a low barrier, the enol form rapidly transforms into the S_1 keto configuration, hereinafter denoted as K^*. An equilibrium rapidly establishes between E^* and K^* through k_{PT} and k_{-PT} while both forms also decay through other relaxation channels (k_E and k_K). The kinetic model described above can be solved exactly for the two excited-state tautomers:

$$N_E(t) = \frac{N_E(0)}{k_a - k_b}\left[(k_a - k_c)\exp(-k_a t) + (k_c - k_b)\exp(-k_b t)\right],$$

$$N_K(t) = \frac{N_E(0)\,k_{PT}}{k_a - k_b}\left[\exp(-k_b t) - \exp(-k_a t)\right],$$

where

$$k_a = \tfrac{1}{2}\left(k' + \sqrt{k'^2 - 4k''}\right),$$

$$k_b = \tfrac{1}{2}\left(k' - \sqrt{k'^2 - 4k''}\right),$$

$$k_c = k_{-PT} + k_K,$$

and

$$k' = k_{PT} + k_{-PT} + k_E + k_K,$$

$$k'' = k_{PT}k_K + k_E k_K + k_E k_{-PT}.$$

$N_E(t)$ and $N_K(t)$ denote the population of E^* and K^*, respectively. Note that k_E and k_K represent the sum of all other radiative and nonradiative decay channels of E^* and K^*, respectively. The total transient current signal as a function of the pump–probe delay time is

$$S(t) = \sigma_E N_E(t) + \sigma_K N_k(t),$$

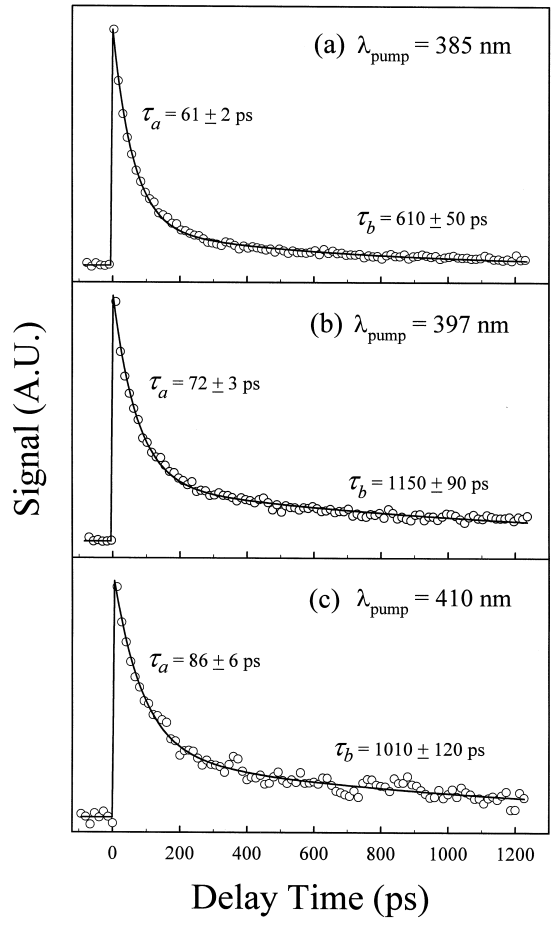

Fig. 2. Long-time transients of HAN excited at three wavelengths: (a) 385 nm, (b) 397 nm and (c) 410 nm. The open circles are experimental data points and the solid lines are results of nonlinear least-square fits to a biexponential decay of the form $A_a\exp(-t/\tau_a) + A_b\exp(-t/\tau_b)$ convoluted with the 200 fs FWHM Gaussian response function. The time constants obtained from the fits are indicated near the corresponding temporal features. The uncertainties are standard errors from fitting a single set of data in each case. The pump and probe pulse energies are the same as those used in Fig. 1 transients. We have also taken intermediate-range scans with smaller step sizes and the analyses yielded eventually the same result for the faster component. Note that the 'initial spike' observed in the early-time transients is not seen here because of the large step size used.

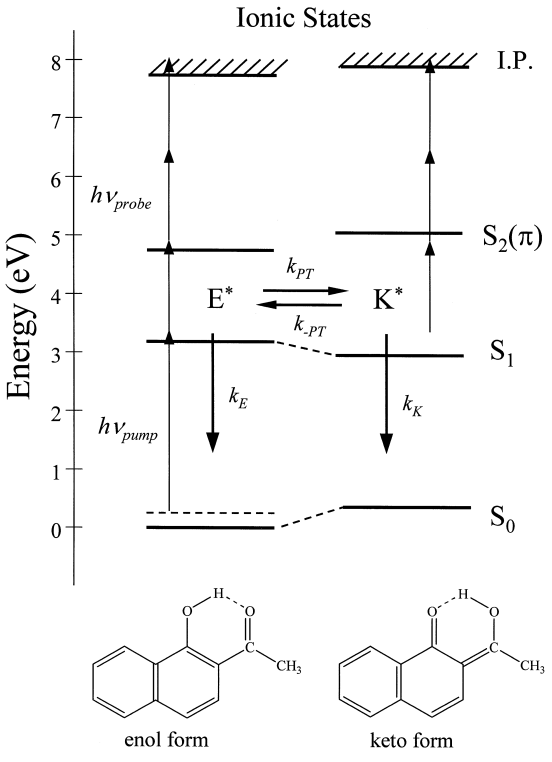

Fig. 3. A schematic energy level diagram of HAN showing the relevant states to the dynamical processes discussed in the text. k_{PT} and k_{-PT} are the rate constants for the forward and reverse ESIPT, respectively. The decay rate constants of the two excited-state tautomers, k_E and k_K, include all other radiative and nonradiative channels excluding ESIPT.

where σ_E and σ_K are factors proportional to the effective ionization cross sections for E^* and K^* by the probe laser, respectively. Clearly, the temporal behaviors of the total transient signal detected in our experiment as well as the fluorescence arising from each of the excited-state tautomers observed by Douhal et al. [9] are dictated by two compound rate constants k_a and k_b. Since neither the initial decay of enol-emission nor the initial rise of keto-emission was observed, Douhal et al. [9] proposed that the equilibrium between E^* and K^* is established much faster than the decay of both tautomers through other channels. Under this assumption ($k_{PT} + k_{-PT} \gg k_E$, k_K) the two compound rate constants become $k_a \approx k_{PT} + k_{-PT}$ and $k_b \approx (k_E + k_K)/2$, i.e., a fast component that is mainly due to the ESIPT relaxation time and a slower component arising mostly from the averaged rates of E^* and K^* decay. This is, of course, consistent with the results reported by Douhal et al. [9]. The $\exp(-k_b t)$ terms in $N_E(t)$ and $N_K(t)$ give rise to the identical fluorescence lifetimes of 9.3 ns emitting from both E^* and K^* when HAN is excited to the S_1–S_0 origin in their experiments [9]. The $\exp(-k_a t)$ term is related to the much faster proton transfer time of few tens of ps, as discussed below, and could not be resolved by their ~ 6 ns instrumental response.

Douhal et al. also found that no enol-emission can be observed at excess energies above ~ 300 cm^{-1} and attributed this observation to a low energy barrier to ESIPT [9]. This implies that the E^*–K^* equilibrium strongly favors the keto-configuration at energies higher than 300 cm^{-1}, i.e., $k_{PT} \gg k_{-PT}$. Above this energy almost all E^* rapidly transform into K^* such that no appreciable enol-emission can be detected. In the present study, the large thermal energy [1] of $\sim 2{,}100$ cm^{-1} and the excitation wavelengths place average excess energies (E_{av}) of $\sim$ 750, 1,550 and 2,330 cm^{-1} above the S_1 zero-point level for the three excitation wavelengths studied. Although these numbers are subjected to some uncertainties, the average excess energy is likely to be above 300 cm^{-1}. Thus, to account for our results at these rather high excess energies, it is appropriate to make the following approximations: $k_{PT} \gg k_{-PT} \approx 0$ and $k_{PT} \gg k_E$, k_K. These simplify the kinetic model into a simple consecutive reaction. The transient signal is then reduced to the following form

$$S(t) \approx N_E(0)\left[(\sigma_E - \sigma_K)\exp(-k_a t) + \sigma_K \exp(-k_b t)\right],$$

where $k_a \approx k_{PT}$ and $k_b \approx k_K$. In the case of $\sigma_E > \sigma_K$, the transient becomes a simple biexponential decay function. The sum of E^* decay and K^* rise (with a lower detection efficiency) results in the faster decay (k_a) which directly gives the proton-transfer time, whereas the slower component (k_b) simply repre-

[1] The average thermal vibrational energy (E_{therm}) was calculated using Gaussian 94 program at the HF/6-31G(d) level with the scaling factor correction for the vibrational frequencies. The average excess energy was then calculated as $E_{av} = E_{h\upsilon} + E_{therm} - E_{0,0}$, where $E_{h\upsilon}$ is the excitation energy and $E_{0,0}$ is the transition energy of the S_1–S_0 origin at 388.6 nm.

sents the decay of K^* through other radiative and nonradiative channels. As shown in Fig. 2, the observed transients are indeed well fitted to biexponential decay functions and no initial rise in fs time scales can be resolved (see Fig. 1). We have also taken scans with intermediate time scales and resolutions to ensure that no other temporal features are present. The time constants $\tau_a = 1/k_a$ and $\tau_b = 1/k_b$ obtained from nonlinear least-square fits are indicated in Fig. 2. Note that even without making any approximation the kinetic model still predicts a biexponential decay as long as the contribution from the E^* decay is greater than that from the K^* rise. Thus, the ESIPT time constants in HAN (S_1) at the energies studied are $\sim$60–85 ps. The initial wave packet prepared by the fs excitation should dephase much faster than these rates and therefore give rise to the observed exponential population evolution. The observed reaction time scale of few tens of ps suggests that there is an energy barrier along the ESIPT reaction coordinate. The slow components decay in $\sim$1.1–0.6 ns and are assigned to the keto form lifetimes. Note that these τ_b's reported here are probably subjected to larger uncertainties than those indicated in Fig. 2 due to the limited scan range of our translation stage ($\sim$1.3 ns). In the ns study [9], the keto form fluorescence lifetime was found to slowly decrease from 9.3 ns at the zero-point level to 7.2 ns at 307 cm^{-1}. At $\sim$830 cm^{-1} the fluorescence became shorter than their laser pulses ($\sim$6 ns) but still observable. Above 900 cm^{-1} the fluorescence was not detectable [9]. Hence, if the energy dependence and the uncertainty due to the limited scan range are taken into account, the $\sim$1.1–0.6 ns keto-form lifetimes observed here are in fact qualitatively consistent with the fluorescence lifetimes reported by Douhal et al. [9].

The lowering of the ionization cross section when E^* transforms into K^* can be justified by the following reasons. Based on the probe–laser irradiance dependence of the transient signal, the initially prepared E^* is probably ionized by absorbing at least three probe photons (see Fig. 3). The first-photon absorption of this three-photon ionization probing is in fact resonant with the second $^1(\pi, \pi^*)$ state, hereinafter denoted as $S_2(\pi)$, of HAN in the enol form. As can be seen in the absorption spectrum shown in Fig. 1(a), the onset of the $S_2(\pi) \leftarrow S_0$ band is near 270 nm. The same transition has been observed and assigned in OHBA [16] and other related molecules [17] in similar spectral regions. Thus, the first probe-photon absorption of E^* can reach the bottom of the enol-form $S_2(\pi)$ state (see Fig. 3). This resonance condition enhances the overall probing efficiency for the enol configuration. Two effects may reduce this enhancement as the configuration changes to the keto form. First, since the potential energy minimum of K^* is expected to be lower than that of E^*, the excited keto tautomer is formed at a higher vibrational excitation. Thus, the first-photon absorption which only reach the bottom of the $S_2(\pi)$ may have a poorer Franck–Condon overlap for K^*. Second, the keto form of the $S_2(\pi)$ state in OHBA has been shown experimentally to be higher in energy than its enol form [12]. Hence, the Franck–Condon overlap for the HAN K^* probing could be further reduced if the HAN $S_2(\pi)$ keto form is also higher in energy than its enol form. In the extreme case, the energy gap between the keto-form S_1 and $S_2(\pi)$ states may become so large such that the first-photon absorption of K^* is no longer resonant with $S_2(\pi)$ but relied on much weaker non-resonant terms. This would make the entire 3-photon ionization cross section much lower for K^*. Similar effects may occur in the final ionization step if the keto from has a higher ionization potential.

We have also considered alternative interpretations to the observed transients. For example, the initially excited singlet E^* may rapidly decay to the nearby triplet states through intersystem crossing (ISC) or to the highly vibrationally excited region of S_0 through internal conversion (IC). In both cases, fast decay reflecting the dynamics of these nonradiative processes can be observed in pump–probe ionization experiments. In the so-called 'intermediate case', ISC is reversible and it is well-known that coherent excitation to the S_1 manifold can lead to a biexponential decay behavior similar to the transients reported here [18]. Although plausible, the typical singlet-triplet splitting in (π, π^*) states of aromatic molecules [19] and the relatively large size of HAN make this assignment highly unlikely. On the other hand, in the 'large-molecule limit', ISC is dissipative and single exponential decay is expected. Evidently, this is not consistent with our observations of biexponential decay for HAN. In fact, if the fast decay of

few tens of ps were due to any nonradiative channel leading to non-fluorescing states, e.g., ISC and IC, then it would reduce the fluorescence quantum yield of HAN (S_1) to an undetectable level for ns fluorescence experiments without photon-counting detection. The fact that Douhal et al. [9] observed fluorescence even at 830 cm^{-1} suggests that the fast decay observed here is not due to ISC or IC. In our ESIPT model, ISC and IC are included in the nonradiative decay channels occurring in both excited enol and keto tautomers.

The results presented here revealed that ESIPT takes place in HAN in few tens of ps in the gas phase, suggesting the existence of a barrier to tautomerization in its S_1 state. On the contrary, a previous gas-phase fs study of methyl salicylate (MS) has shown that ESIPT occurs in ~ 60 fs at an excess energy of $\sim 3{,}900$ cm^{-1}, implying a barrierless route to tautomerization [6]. The presence of the electron-donating group OCH_3 in MS may play a role in determining the ESIPT dynamics. In the case of the benzene analogues of HAN, i.e., OHBA and *o*-hydroxyacetophenone (OHAP), no gas-phase time-resolved studies have been reported to the best of our knowledge. However, a distorted single minimum potential energy surface has been inferred based on the broad and structureless absorption spectra of OHBA S_1–S_0 transition observed in gas cells [20] as well as in supersonic jets [21]. Ab-initio calculations of OHBA [22] and OHAP [23] have predicted that the 'bright' $S_1(\pi, \pi^*)$ state has no barrier to ESIPT, whereas the nearly 'dark' and isoenergetic $^1(n, \pi^*)$ state possesses a substantial barrier. On the other hand, ps fluorescence measurements for OHBA and OHAP in nonpolar solvents at 77 K have shown that ESIPT occurs in ~ 830 and ~ 90 ps, respectively [24]. Clearly, there are some discrepancies among these data and more gas-phase studies of OHBA and OHAP are needed for further comparisons.

The observed ESIPT rate constants in HAN slowly increase from $1/85$ ps^{-1} at $E_{av} \approx 750$ cm^{-1} to $1/60$ ps^{-1} at $E_{av} \approx 2{,}330$ cm^{-1}. The 385 nm excitation is near the origin of the HAN S_1–S_0 transition, hence the initial vibrational energy distribution in E^* should resemble the ground-state thermal distribution at 45°C. For longer pump wavelengths at 397 and 410 nm, the excitations are due to hot band absorption and reach even lower energy regions of the excited state surface. These imply that only those low-frequency modes can be significantly populated in E^* in all cases. The chelate ring bound by the relatively loose intramolecular hydrogen bond provides many low-frequency modes including various in- and out-of-plane motions of the C–OH and C–C = O groups as well as the hindered rotation of the CH_3 group [9,23]. Thus we have a rather loose but more energetic chelate ring that is attached to the more rigid but cold aromatic ring system, i.e., the excess energy is mostly localized in the chelate ring system where the ESIPT occurs. Intramolecular vibrational energy redistribution (IVR) among these low-frequency modes should be facile even at the lowest excess energy studied due to their similar frequencies and the high density of states made up mainly by these low-frequency modes. While the system is seeking for the exit, the various chelate ring motions modulate the barrier height and the reaction barrier can be overcome when enough energy is channeled into the reaction coordinates. The observed reaction time scales and the smooth energy dependence are consistent with the picture described above and the proposal of a low energy barrier. One should also note that the broad thermal distribution of the ground state could blur the excess energy dependence to some extent. Similar studies carried out in supersonic jets can remove the thermal congestion and are being planned for HAN and other related molecules in this laboratory.

4. Conclusions

We have employed femtosecond time-resolved multiphoton ionization spectroscopy to investigate the excited-state dynamics in HAN. The transient signal of the excited HAN exhibits a biexponential decay behavior that can be consistently interpreted in terms of rapid ESIPT occurring in HAN (S_1). The analyses revealed that, upon photoexcitation to its S_1 state, HAN undergoes rapid tautomerization in $\sim$ 60–85 ps at the energies studied followed by other much slower radiative and non-radiative decay processes in ns to sub-ns time scales. The reaction time scales suggest the existence of an energy barrier to tautomerization on the HAN (S_1) potential energy surface.

Acknowledgements

This work was supported by a grant (NSC88-2113-M-007-037) from the National Science Council of the Republic of China.

References

[1] E.F. Caldin, V. Gold (Eds.), Proton Transfer Reactions, Chapman and Hall, London, 1975.
[2] P.F. Barbara, M. Nicol, M.A. El-Sayed (Eds.), Photoinduced Proton Transfer in Chemistry, Biology and Physics, J. Phys. Chem. 95 (1991) 10215.
[3] P.F. Barbara, P.K. Walsh, L.E. Brus, J. Phys. Chem. 93 (1989) 29.
[4] A. Weller, Z. Elektrochem. 60 (1956) 1144.
[5] P.F. Barbara, H.P. Trommsdorff (Eds.), Spectroscopy and Dynamics of Elementary Proton Transfer in Polyatomic Systems, Chem. Phys. 136 (1989) 163-360.
[6] J.L. Herek, S. Pedersen, L. Bañares, A.H. Zewail, J. Chem. Phys. 97 (1992) 9046.
[7] B.J. Schwartz, L.A. Peteanu, C.B. Harris, J. Phys. Chem. 96 (1992) 3591.
[8] J. Catalán, J.C. del Valle, J. Am. Chem. Soc. 115 (1993) 4321.
[9] A. Douhal, F. Lahmani, A. Zehnacker-Rentien, Chem. Phys. 178 (1993) 49.
[10] S. Tobita, M. Yamamoto, N. Kurahayashi, R. Tsukagoshi, Y. Nakamura, H. Shizuka, J. Phys. Chem. A 102 (1998) 5206.
[11] S. Pedersen, L. Banares, A.H. Zewail, J. Chem. Phys. 97 (1992) 8801.
[12] W. Fuß, T. Schikarski, W.E. Schmid, S.A. Trushin, P. Hering, K.L. Kompa, J. Chem. Phys. 106 (1997) 2205.
[13] A. Douhal, S.K. Kim, A.H. Zewail, Nature 378 (1995) 260.
[14] G. Grégoire, I. Dimicoli, M. Mons, C. Dedonder-Lardeux, C. Jouvet, S. Martrenchard, D. Solgadi, J. Phys. Chem. A 102 (1998) 7896.
[15] N.F. Scherer, L.R. Khundkar, T.S. Rose, A.H. Zewail, J. Phys. Chem. 91 (1987) 6478.
[16] S. Nagaoka, U. Nagashima, Chem. Phys. 136 (1989) 153.
[17] S. Nagaoka, Y. Shinde, K. Mukai, U. Nagashima, J. Phys. Chem. 101 (1997) 3061.
[18] J. Kommandeur, W.A. Majewski, W.L. Meerts, D.W. Pratt, Annu. Rev. Phys. Chem. 38 (1987) 433.
[19] S.P. McGlynn, T. Azumi, M. Kinoshita, Molecular Spectroscopy of the Triplet State, Prentice-Hall, Englewood Cliffs, NJ, 1969.
[20] C.J. Selisker, J. Mol. Spectrosc. 53 (1974) 140.
[21] S. Nagaoka, U. Nagashima, N. Ohta, M. Fujita, T. Takemura, J. Phys. Chem. 92 (1988) 166.
[22] A.L. Sobolewski, W. Domcke, Chem. Phys. 184 (1994) 115.
[23] M.V. Vener, S. Scheiner, J. Phys. Chem. 99 (1995) 642.
[24] S. Nagaoka, N. Hirota, M. Sumitani, K. Yoshihara, J. Am. Chem. Soc. 105 (1983) 4220.